

Article

Stimuli-Sensitive Aggregation-Induced Emission of Organogelators Containing Mesogenic Au(I) Complexes

Supattra Panthai , Ryota Fukuhara, Kyohei Hisano  and Osamu Tsutsumi * 

Department of Applied Chemistry, Ritsumeikan University, 1-1-1 Nojihigashi, Kusatsu 525-8577, Japan; gr0344hv@ed.ritsumeikan.ac.jp (S.P.); r.f.car1025@gmail.com (R.F.); hisano@fc.ritsumeikan.ac.jp (K.H.)

* Correspondence: tsutsumi@sk.ritsumeikan.ac.jp

Received: 22 April 2020; Accepted: 7 May 2020; Published: 9 May 2020



Abstract: As the luminescence from conventional organic luminophores is typically quenched in constrained environments, the aggregation-induced emission (AIE) phenomenon is of interest for the development of materials that exhibit strong luminescence in condensed phases. Herein, new bismesogenic Au complexes were developed as organogelators and their photophysical properties, including their AIE characteristics, were investigated in organogels and crystals. The crystals of the gold complexes exhibited room-temperature phosphorescence with relatively high quantum yields. Moreover, the gold complexes also showed photoluminescence in the organogels and we demonstrated that the reversible switching of the luminescence intensity was induced by the sol-gel phase transition. The intense photoluminescence in the crystal and gel was induced by the restricted internal motion of the luminophore in the molecular aggregates. However, in the sol, the network structure of the organogel was destroyed and the nonradiative deactivation of the excited states was enhanced. As a result, we can conclude that the switching of the luminescence intensity was induced by changes in the aggregated structures of the molecules. The developed Au-complex-based gelators are excellent candidates for the realization of stimuli-responsive soft and smart luminescent materials.

Keywords: Au complex; organogel; sol-gel transition; aggregation-induced emission

1. Introduction

Strong luminescence from organic materials has been receiving growing interest for its applications in light-emitting devices, chemical sensors and bioimaging materials [1–3]. However, the luminescence from conventional organic luminophores suffers in concentrated solutions or condensed phases owing to the aggregation-caused quenching effect. In recent years, Tang and co-workers have developed efficient luminescent materials that exhibit intense luminescence in condensed phases via a phenomenon known as aggregation-induced emission (AIE) [4,5]. This phenomenon is caused by the restriction of internal motions in molecules, namely, rotations and vibrations by aggregation, which results in the nonradiative deactivation of the excited molecules. Thus, the photoluminescence properties of AIE materials strongly depend on the aggregated structures as well as the primary structures of molecules.

Various d^{10} transition metal complexes exhibit AIE behavior. For instance, Au(I) complexes are known to be AIE-active materials and in the past decade, many groups have reported the AIE behavior of Au complexes [6–10]. In our previous studies, various Au complexes were found to show efficient room-temperature phosphorescence (RTP) with a quantum yield (Φ) of >50% in a crystalline state under ambient conditions [11–14]. Uniquely, in Au complexes, intermolecular interactions occur between Au atoms (aurophilic interactions) and their highly emissive properties in condensed phases have been attributed to these aurophilic interactions [10,15–19]. An aurophilic interaction is formed

when the interatomic distance between Au atoms becomes less than 3.6 Å, that is, shorter than the sum of the van der Waal radii of two Au atoms (3.8 Å) [10,16,17]. Numerous studies have reported that the photoluminescence behavior of Au complexes in condensed phases depends on the intermolecular Au–Au distances [20–30].

AIE is usually observed in rigid solids like crystals; however, several groups have also reported the occurrence of AIE phenomena in soft condensed phases, e.g., liquid crystal (LC) phases [31,32], noncrystalline polymers [33,34], and so on [35,36]. In particular, LC gold complexes have been reported to show changes in emission behavior through phase transitions [37,38]. LCs are self-organized soft materials and the aggregated structures in LC phases can be easily controlled by external stimuli. Thus, several mesogenic Au complexes have been developed and their AIE and LC behaviors have been reported [11–13]. For example, AIE-active LC Au complexes with rod-like molecular structures (e.g., pentylisocyno 2-(4-(hexyloxy)phenyl)ethynylgold(I) (**R6**), Figure 1) have been studied [11]. In such materials, the Au complex acts as both a mesogen and a luminogen. We reported that these complexes formed dimers in the crystalline, LC and in isotropic phases owing to the strong interactions between the gold atoms of neighboring molecules, and that these dimers exhibited intense blue photoluminescence in the condensed phases. We observed that the luminescence properties, vis., luminescence color and intensity, of mesogenic Au complexes can be tuned by crystalline–LC and LC–isotropic phase transitions [11–13,38]. Namely, the mesogenic Au complexes showed both AIE behavior and a high sensitivity of the luminescence to their aggregated structure. Therefore, we considered that the mesogenic Au complexes could be useful building blocks for creating luminescent soft materials with sensitive luminescence behavior to external stimuli.

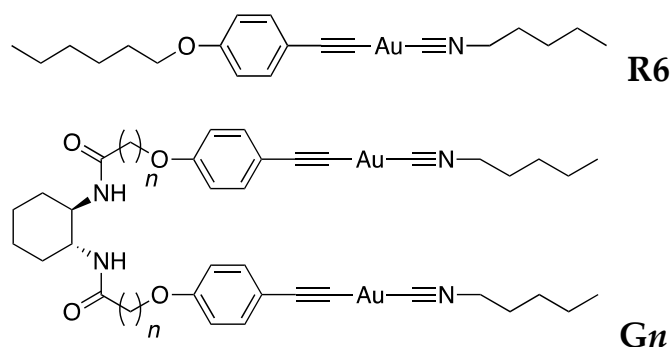


Figure 1. Molecular structures of **R6** and **Gn** ($n = 5, 10$).

Inspired by our previous work, in this study, we designed bimesogenic Au complexes with alkyl spacers of different lengths (**Gn**, Figure 1), and evaluated their photophysical properties by comparison with previously reported LC Au complex **R6**. Interestingly, we found that these new Au complexes showed gel-formation properties in common organic solvents. In gels, similarly to the LC phases, molecules formed “soft” aggregates via an exquisite balance in intermolecular interactions between the gel-forming molecules (gelators) and the solvation with the solvent molecules. Owing to this aggregation, it was expected that AIE phenomena will still be observed in gels [39–47]. However, as the gels are soft molecular aggregates, the aggregated structure can be easily controlled by various external stimuli; thus, AIE gelators have potential applications as excellent stimuli-responsive luminescent materials [48–57]. In this paper, we discussed the relationship between the aggregated structures of molecules and the luminescence behavior of synthesized gold complexes **Gn**. Notably, we found that the luminescence behavior of the Au complexes in organogels can be reversibly switched on and off through the gel–sol phase transition.

2. Results and Discussion

Au complexes **Gn** were newly synthesized from the corresponding ethynylbenzene derivatives [11]. The prepared complexes were fully characterized and the analytical data confirmed that the desired complexes were obtained. The preparation details and the related characterization data are provided in the Materials and Methods and the Supplementary Materials (Scheme S1 and Figures S1 and S2).

While purifying the obtained complexes by recrystallization, we found that the complexes formed organogels in some solvents. Thus, we examined the gelation abilities of the complexes in various solvents. The gelation behavior of **Gn** in various solvents and solvent mixtures is summarized in Table 1. The complexes with longer alkyl spacers (**G5** and **G10**) formed gels in several solvents (Figure 2a,b), depending on the polarity of the solvent system. These results indicated that a certain spacer length was required to form a gel and that the versatility of the gelled solvent was improved as the spacer length increased. It is likely that the intermolecular interactions between the alkyl groups (van der Waals force), as well as hydrogen bonding, were important for the formation of molecular assemblies in the gels. Hanabusa et al. reported that a cyclohexane diamide with long alkyl chains showed a very high gelling ability [58]. Because the present complexes contained a cyclohexane diamide moiety, it was reasonable that the complexes with longer alkyl spacers showed better gelation properties. Moreover, the introduction of Au(I) to these complexes was expected to result in relatively strong intermolecular interactions, i.e., Au–Au interaction, which could have a positive effect on gelation [59,60]. However, the steric hindrance of the complexes could weaken van der Waals interactions between the alkyl chains and inhibit the stacking of the cyclohexane diamide moieties. These negative steric effects, which can interrupt gelation, were anticipated to be more prominent in the compound with the shorter spacer.

Table 1. Gel-formation tests for **Gn** in various solvents.

Solvent (v/v)	G5	G10
Hexane	IS	IS
Hexane/CH ₂ Cl ₂ (1/2)	G	S
Hexane/CH ₂ Cl ₂ (2/3)	–	G
CH ₂ Cl ₂	S	S
THF	P	G
EtOAc/CH ₂ Cl ₂ (1/2)	G	S
EtOAc/CH ₂ Cl ₂ (2/3)	–	G
EtOAc	IS	IS
Hexane/CHCl ₃ (1/2)	G	S
Hexane/CHCl ₃ (2/3)	PG	G
CHCl ₃	S	S
EtOH	IS	IS
CH ₃ CN	IS	IS
DMF	S	S

Abbreviations: G, gel; IS, insoluble at the boiling point of the solvent; S, solution at 20 °C; P, precipitate; PG, partial gel; –, not tested.

The gels formed by **G5** in hexane/CHCl₃ (1/2, v/v) and **G10** in hexane/CHCl₃ (2/3, v/v) were air-dried and the microstructures of the obtained xerogels were observed by scanning electron microscopy (SEM), as shown in Figure 2c,d. Micrometer-scale fibrous aggregates were observed for both xerogels, although a larger fiber diameter was observed for the complex with the longer alkyl chain length (**G10**). We considered this increase in fiber diameter to be the result of stronger van der Waals interactions between the longer alkyl chains.

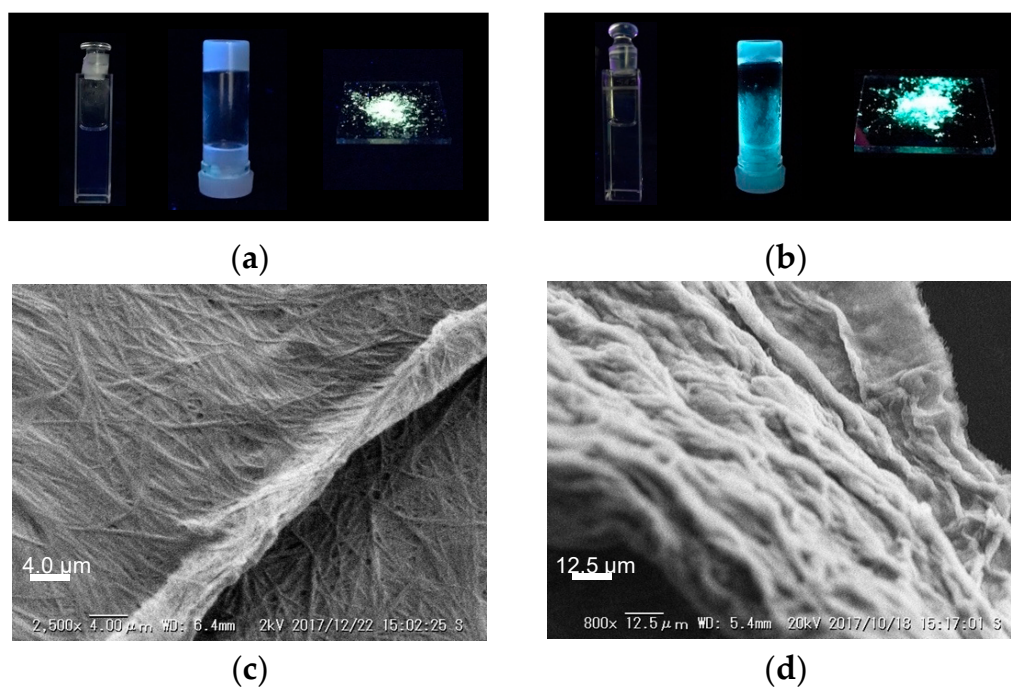


Figure 2. Photographs of the complexes (a) **G5** and (b) **G10** in a CH_2Cl_2 solution ($1.0 \times 10^{-6} \text{ mol L}^{-1}$, left), in gels (hexane/ CHCl_3 (1/2, v/v) for **G5** and hexane/ CHCl_3 (2/3, v/v) for **G10**; 10 mg mL^{-1} , middle), and in crystals (right) taken under UV irradiation at 365 nm. Scanning electron microscopy (SEM) images of the (c) **G5** and (d) **G10** xerogels obtained from the organogels.

The photophysical properties of complexes **G5** and **G10** were observed as representative examples. Figure S3 shows the UV-Vis absorption spectra of the complexes in dilute CH_2Cl_2 solutions ($1.0 \times 10^{-5} \text{ mol L}^{-1}$). In dilute solutions, all the complexes exhibited similar spectra shapes with the absorption maxima at 288 nm. This result implied that the luminescent centers of the complexes had the same electronic structure; therefore, the structural differences in the spacer length did not affect the electronic structure. At the absorption maxima, all the complexes showed large molar extinction coefficients of $>10^4 \text{ L mol}^{-1} \text{ cm}^{-1}$ (5.5×10^4 and $5.2 \times 10^4 \text{ L mol}^{-1} \text{ cm}^{-1}$ for **G5** and **G10**, respectively). Thus, this absorption band could be assigned to a fully allowed $\pi-\pi^*$ transition.

Complexes **G5** and **G10** showed photoluminescence at 360 nm even in dilute solutions (Figure 3 and Figure S3). In contrast, the complex **R6** was reported to exhibit no photoluminescence in dilute solutions ($<10^{-4} \text{ mol L}^{-1}$) but weak luminescence in relatively concentrated solutions [38]. This behavior occurred because the luminescence of **R6** originated from the molecular aggregates formed by intermolecular Au–Au interactions. However, as the present complexes contained a pair of luminogens, the molecules could form luminescent aggregates even in dilute solutions. In Figure S6, the 3D model of the **5G** molecule optimized by a semiempirical calculation using PM6 is shown as a representative example. The model indicated that the two Au atoms in the **5G** molecule were separated by $>10 \text{ \AA}$ in the ground state. However, we could consider that the luminogens formed excimer-like aggregates by the Au–Au interaction in the excited state, and we could conclude that this aggregate luminesced in the dilute solution.

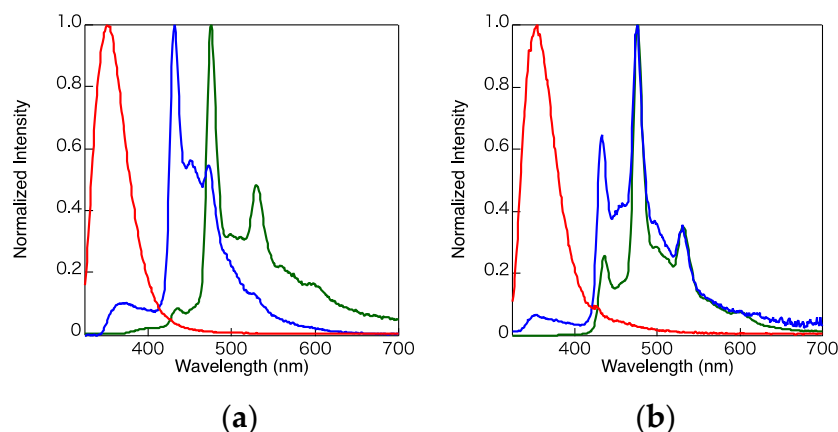


Figure 3. Photoluminescence spectra ($\lambda_{\text{ex}} = 288$ nm) for (a) **G5** and (b) **G10**; red, in a CH_2Cl_2 solution (1.0×10^{-6} mol L^{-1}); blue, in the gel phase (10 mg mL^{-1}); and green, in the crystals.

Figure 3 also shows the photoluminescence spectra of the complexes in crystals. In the crystals, **G5** and **G10** strongly emitted green and bluish-green photoluminescence, respectively (Figure S4a,b), and three major emission bands were observed at 430, 475 and 530 nm. To obtain more information about the photoluminescence properties, we measured the luminescence lifetimes (τ) of both complexes in the crystals in the wavelength range between 400 and 700 nm. Biexponential luminescence decays were observed for the crystals of both complexes (Figure 4), with τ values in the order of submicroseconds and microseconds (Table 2), indicating that the observed luminescence was phosphorescence. In contrast, mono-luminogenic complex **R6** was reported to show a monoexponential decay [38]. As mentioned above, several emission bands were observed in the luminescence spectrum of the crystals of the **G n** complexes, implying the presence of two or more excited states and thus, they exhibited biexponential decay profiles. The luminescence quantum yield (Φ) was also measured for both complexes. In the crystals, the complexes exhibited relatively high Φ values at room temperature in air (Table 2), although the luminescence was phosphorescence. This was the same phenomenon as that observed by Tang and co-workers, which is known as crystallization-induced phosphorescence [61,62].

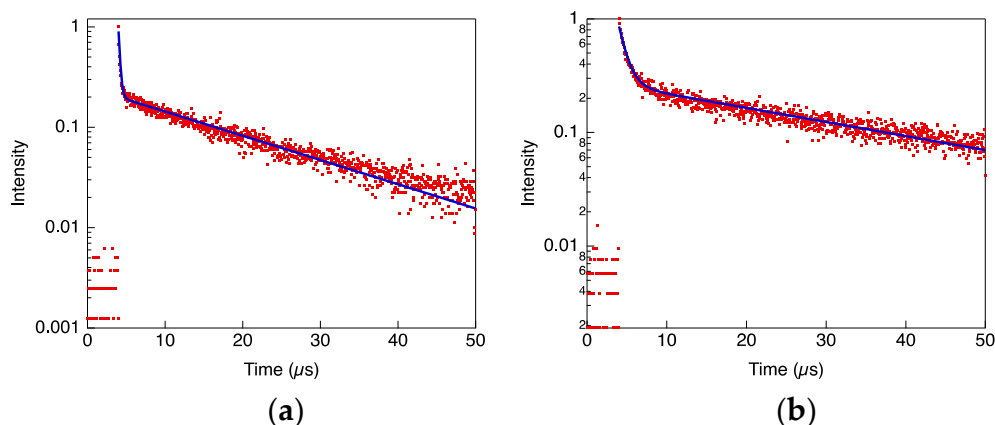


Figure 4. Luminescence decay profiles of (a) **G5** and (b) **G10** in the crystals at ambient temperature; red, observed decay; blue, fitting curve.

Table 2. Photoluminescence lifetimes and the quantum yields of **G*n*** complexes in the crystals determined at room temperature in air.

Complex	Lifetime, τ (μ s)	Quantum Yield, Φ (%)
G5	0.23 (74%)	1.9
	19 (26%)	
G10	1.1 (72%)	16
	38 (28%)	

The complexes also luminesced in gels (Figure 3). For the **G5** gel, the observed luminescence spectrum was different from those in the solution and in the crystal. However, for the **G10** gel, the luminescence spectrum was similar to that in the crystal, except that the relative intensity of the luminescence band at 430 nm was greater in the gel. For both complexes, a comparison of the emission spectra in the gels and the crystals revealed that a small emission band at approximately 350 nm was only observed in the gels. The maximum wavelength of this emission band was similar to that observed in a dilute solution. Therefore, we could conclude that this emission originated from isolated molecules in the solution.

To further discuss the relationship between the luminescence behavior and the aggregated structure, the temperature dependence of the luminescence of the Au complexes was observed (Figures 5 and 6). During the heating process, the luminescence intensity gradually decreased (Figure 5a,c and Figure 6 (top)). Molecular motions, e.g., vibrations and rotations around covalent bonds, which deactivate the excited states of the luminogens, were activated at higher temperatures; therefore, this gradual change is a very common phenomenon in luminescent materials. In contrast, during the cooling process, an abrupt increase in the luminescence intensity occurred at 40 °C (Figure 5b,d and Figure 6 (middle)). The reversible sol-gel phase transition occurred between 35 °C and 40 °C, as shown in the photographs in Figure 6 (bottom); thus, this abrupt change in the luminescence intensity was due to a change in the aggregated structure brought about by the phase transition. We have previously reported that a sudden disappearance of luminescence was induced by the crystal-to-isotropic phase transition in some Au complexes, because the luminescent aggregates were destroyed in the isotropic phase [63]. Namely, this “on–off” switching of photoluminescence by phase transition resulted from the sensitivity of the luminescence to its aggregated structure. Similar to previously reported complexes in the isotropic phase, in the sol, the network structure of the organogel was destroyed and the micro-Brownian motion of the luminogens, which enhanced the nonradiative deactivation of the excited states, was activated. Consequently, as shown by the results in Figure 5b,d, a significant increase in the luminescence intensity accompanied the sol-gel phase transition in both **G5** and **G10** in the cooling process. On the other hand, in the heating process, the sharp change in the luminescence intensity at the sol-gel phase transition temperature was not observed. Generally, the sol-gel transition of this type of low-molecular-weight organic gelators is not a sharp transition like the crystalline–isotropic transition. In addition, due to the low thermal conductivities of glass vials and organic solvents, the temperature of the system is inhomogeneous depending on the heating and cooling rate. We considered that this was the reason for the lack of sharp change in the luminescence intensity at the sol-gel phase transition temperature in the heating process shown in Figure 6 (top) for both complexes. This luminescence intensity change was observed to be reversibly induced by the phase transition (Figure 5 and Figure S5), and this result also supported that the phenomenon was due to the change in the aggregated structure brought about by the reversible sol-gel phase transition.

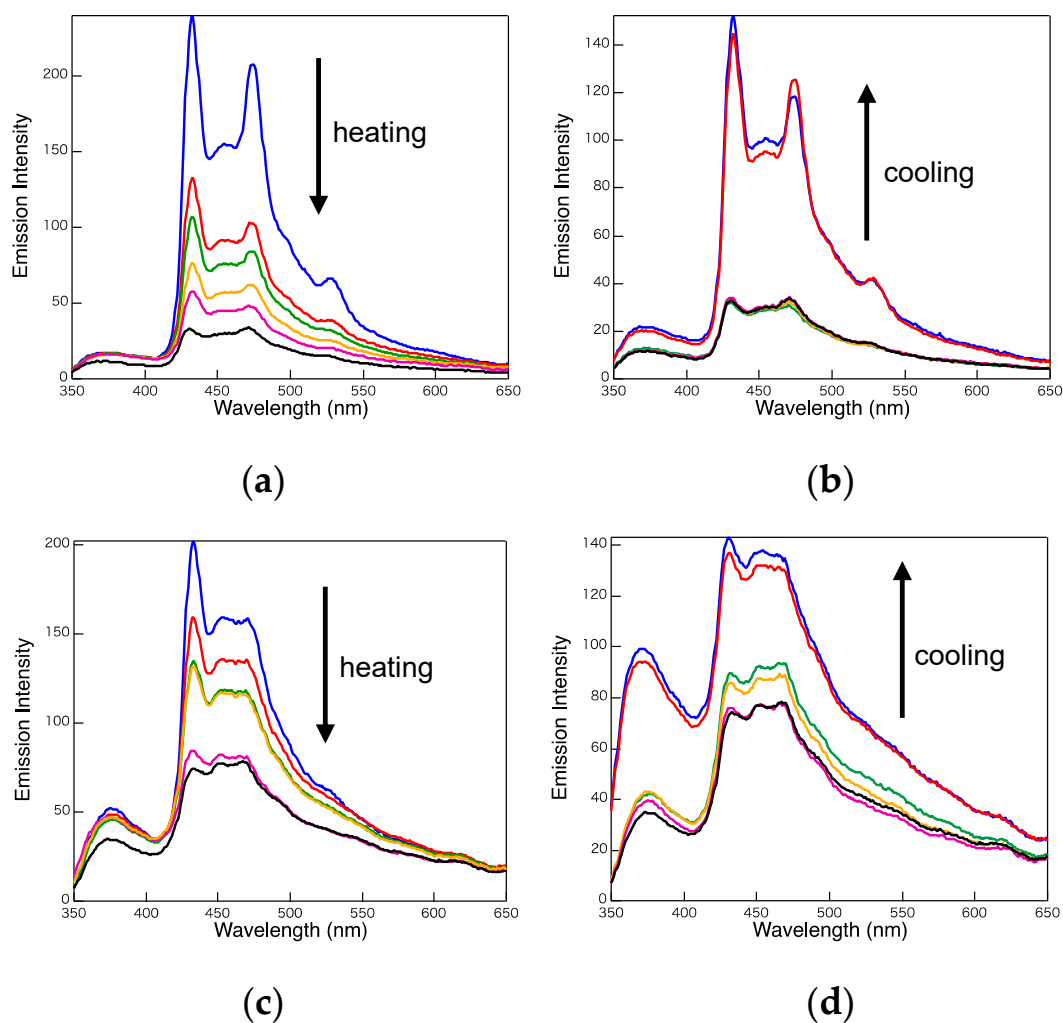


Figure 5. Temperature dependence of the luminescence spectra of the **Gn** complexes in the gel and sol phases (10 mg mL^{-1} , $\lambda_{\text{ex}} = 288 \text{ nm}$): **G5** in hexane/ CHCl_3 ($1/2, v/v$) upon (a) heating and (b) cooling; **G10** in hexane/ CHCl_3 ($2/3, v/v$) upon (c) heating and (d) cooling. The spectra were recorded every $5 \text{ }^\circ\text{C}$ between $30 \text{ }^\circ\text{C}$ and $55 \text{ }^\circ\text{C}$: blue, $30 \text{ }^\circ\text{C}$; red, $35 \text{ }^\circ\text{C}$; green, $40 \text{ }^\circ\text{C}$; orange, $45 \text{ }^\circ\text{C}$; purple, $50 \text{ }^\circ\text{C}$; and black, $55 \text{ }^\circ\text{C}$.

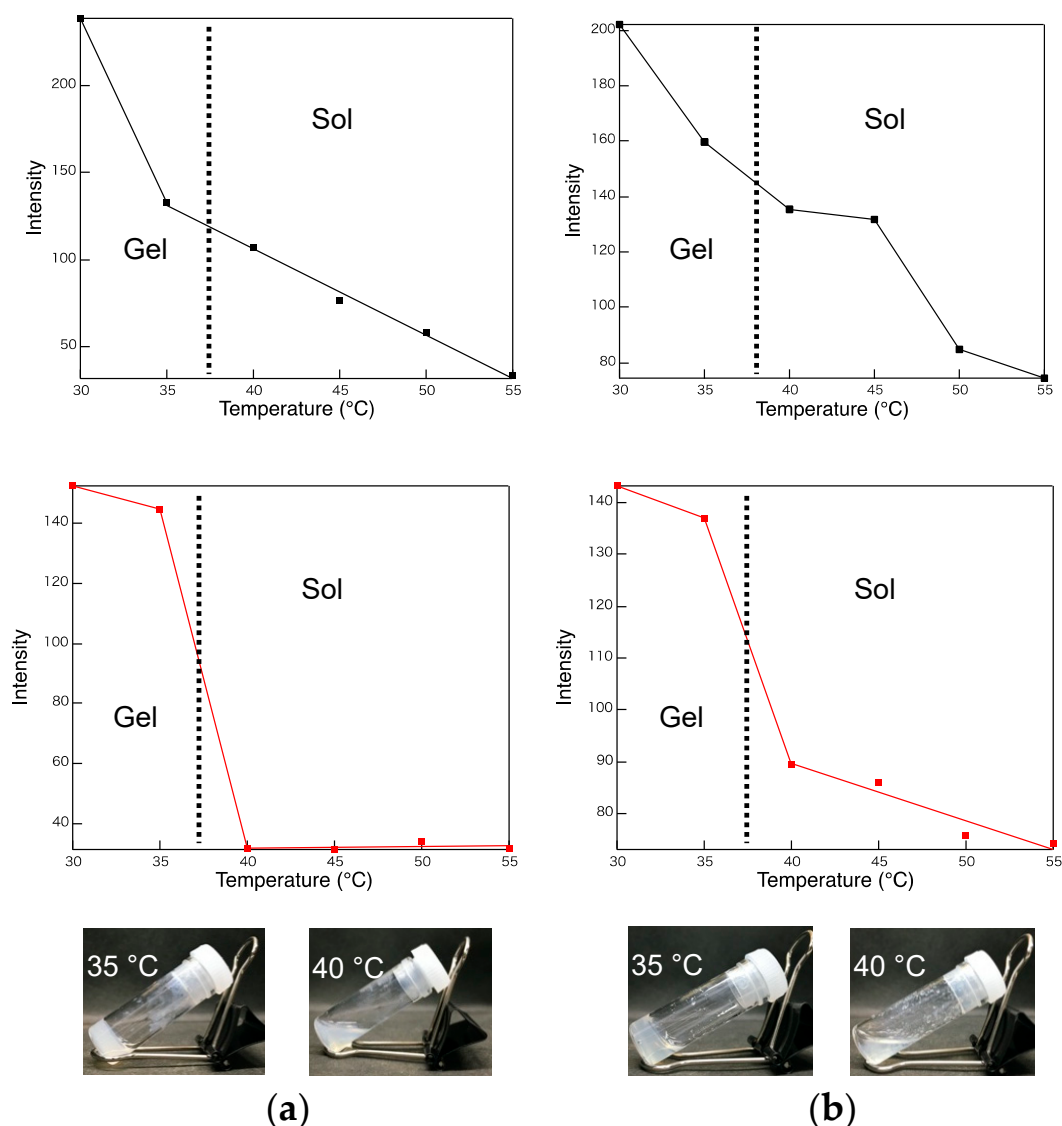


Figure 6. Emission intensity at 430 nm of the **G_n** complexes as a function of temperature in the heating process (top) and cooling process (middle). Photographs of the gel and sol phases at temperatures of 35 and 40 °C, respectively (bottom). (a) **G5** (10 mg mL⁻¹ in hexane/CHCl₃ (1/2, v/v)) and (b) **G10** (10 mg mL⁻¹ in hexane/CHCl₃ (2/3, v/v)).

3. Materials and Methods

3.1. Preparation of Materials

New complexes **G_n** ($n = 5$, and 10) were synthesized according to the synthetic route shown in Scheme S1. The details of the synthetic methods and purification procedures are described in the Supplementary Materials. The structures and purities of the complexes were confirmed by ¹H NMR spectroscopy (Figures S1 and S2), high-resolution mass spectroscopy (HRMS), infrared (IR) spectroscopy and elemental analysis. The ¹H NMR spectra were recorded on a 400 MHz NMR spectrometer (ECS-400; JEOL, Tokyo, Japan) using a residual proton in the NMR solvent as an internal reference. The IR spectra were recorded using the KBr disc method (FT/IR-610; JASCO, Tokyo, Japan). HRMS data were collected using a micrOTOF-QII mass spectrometer (Bruker Daltonics, Billerica, MA, USA).

G5: ¹H NMR (400 MHz, CDCl₃, δ): 7.39 (dd, $J = 6.7, 2.0$ Hz, 4H; 3,5-H in phenyl), 6.75 (dd, $J = 6.7, 2.0$ Hz, 4H; 2,6-H in phenyl), 5.90 (s, 2H; CONH), 3.90 (t, $J = 6.3$ Hz, 4H; OCH₂), 3.62 (m, 6H;

NHCH, NCH₂), 2.10 (t, *J* = 7.3 Hz, 4H; OCH₂CH₂CH₂CH₂CH₂), 2.02 (d, *J* = 12 Hz, 2H; equatorial 2,5-H in cyclohexane), 1.83 (m, 4H; NCH₂CH₂), 1.73 (quin, *J* = 7.0 Hz, 6H; OCH₂CH₂, equatorial 3,4-H in cyclohexane), 1.65–1.57 (m, 4H; OCH₂CH₂CH₂CH₂), 1.47–1.20 (m, 16H; OCH₂CH₂CH₂, 2H; axial 2,5-H in cyclohexane, 2H; axial 3,4-H in cyclohexane, NCH₂CH₂(CH₂)₂), 0.95 (t, *J* = 7.1 Hz, 6H; N(CH₂)₄CH₃). FTIR (KBr): ν = 3286, 2932, 2859, 2245, 1639, 1504, 1243 cm⁻¹. TOF-MS (ESI, *m/z*): calcd for C₄₆H₆₃Au₂N₄O₄ [M + H]⁺, 1129.4175; found, 1129.3689.

G10: ¹H NMR (400 MHz, CDCl₃, δ): 7.38 (dd, *J* = 6.7, 2.0 Hz, 4H; 3,5-H in phenyl), 6.76 (dd, *J* = 6.7, 2.0 Hz, 4H; 2,6-H in phenyl), 5.91 (s, 2H; CONH), 3.91 (t, *J* = 6.5 Hz, 4H; OCH₂), 3.61 (m, 6H; NHCH, NCH₂), 2.10 (t, *J* = 7.3 Hz, 4H; COCH₂), 2.02 (d, *J* = 12.2 Hz, 2H; equatorial 2,5-H in cyclohexane), 1.82 (m, 4H; NCH₂CH₂), 1.73 (quin, *J* = 7.2 Hz, 6H; OCH₂CH₂, equatorial 3,4-H in cyclohexane), 1.65–1.57 (m, 4H; COCH₂CH₂), 1.41 (m, 12H; OCH₂CH₂CH₂, NCH₂CH₂(CH₂)₂), 1.34–1.20 (m, 20H; OCH₂CH₂CH₂(CH₂)₅, 2H; axial 2,5-H in cyclohexane, 2H; axial 3,4-H in cyclohexane), 0.94 (t, *J* = 7.0 Hz, 6H; N(CH₂)₄CH₃). FTIR (KBr): ν = 3285, 2925, 2853, 2247, 1637, 1504, 1243 cm⁻¹. TOF-MS (ESI, *m/z*): calcd for C₅₆H₈₃Au₂N₄O₄ [M + H]⁺, 1269.5740; found, 1269.6100.

3.2. Gelation Ability

To test the gelation ability, the complex **G5** or **G10** (10 mg) was added to 1 mL of solvent (see Table 1 for the tested solvents and solvent mixtures) at room temperature, and then the mixture was heated at the boiling point of the solvent to obtain a homogeneous solution. The solution was then cooled to room temperature, and the gelation was evaluated based on whether the gel formation could be observed in the vessel.

3.3. Photophysical Properties

The UV-Vis absorption spectra were recorded using a V-500 absorption spectrophotometer (Tokyo JASCO, Tokyo, Japan). The steady-state photoluminescence spectra were obtained using a F-7000 fluorescence spectrometer (Hitachi, Tokyo, Japan). The photoluminescence quantum yields were estimated using a calibrated integrating sphere system (Hitachi, Tokyo, Japan). The photoluminescence lifetimes were measured using a Nd:YAG (neodymium-doped yttrium aluminum garnet) laser (Continuum, Minilite II; λ = 355 nm, pulse width = 4 ns (fwhm), repetition rate = 10 Hz) as the excitation source, with the decay profiles recorded using a streak camera (C7700, Hamamatsu Photonics, Hamamatsu, Japan).

4. Conclusions

In summary, new bismesogenic-Au-complex-based organic gelators with AIE characteristics were developed. The gelation ability of these gold complexes depended on the alkyl spacer length between the cyclohexane diamide unit and the Au complex. A longer alkyl spacer enhanced self-assembly through intermolecular interactions to form the organogels. The developed complexes showed photoluminescence even in dilute solutions owing to the aggregation of luminogens induced by intramolecular Au–Au interactions. The crystals of the gold complexes exhibited RTP in the presence of air with relatively high quantum yields. Moreover, the gold complexes showed photoluminescence in the organogels. Notably, in the organogel, we demonstrated that the reversible switching of the luminescence intensity was induced by the sol-gel phase transition. In the condensed phases (crystals and gel), the intense photoluminescence was induced by the restriction of the internal motion of the luminophore in the molecular aggregates. However, in the sol, the network structure of the organogel was destroyed, which improved the nonradiative deactivation of the excited states. As a result, the observed luminescence intensity switching originated from changes in the aggregated structures of the molecules. These stimuli-responsive properties make these Au-complex-based gelators attractive for the development of soft and smart luminescent materials.

Supplementary Materials: The following are available online at <http://www.mdpi.com/2073-4352/10/5/388/s1>, Scheme S1: Synthesis route of **Gn**, Figure S1: ¹H NMR spectrum of **G5**, Figure S2: ¹H NMR spectrum of **G10**, Figure S3: Photophysical properties of complexes **Gn** in dilute solution, Figure S4: Photophysical properties of complexes **Gn** in crystals, Figure S5: Temperature dependence of luminescence spectra during 2nd heating and cooling processes, Figure S6: 3D model of **G5** molecule.

Author Contributions: Conceptualization, O.T.; methodology, S.P., R.F. and K.H.; investigation, S.P., R.F. and K.H.; writing—original draft preparation, S.P.; writing—review and editing, O.T.; visualization, K.H.; project administration, O.T.; funding acquisition, O.T. All authors have read and agreed to the published version of the manuscript.

Funding: This research was supported by JSPS KAKENHI (18K05265 and 18H03764 for OT; 19K21131 for KH), JST A-STEP (JPMJTM19C9), the JICA Collaboration Kick-starter Program (RU/IITH), the Japan–Egypt Research Cooperative Program (JSPS/MOSR-STDF), the Ritsumeikan Global Innovation Research Organization (R-GIRO), and the Cooperative Research Program of the Network Joint Research Center for Materials and Devices (Tokyo Institute of Technology).

Conflicts of Interest: The authors declare no conflict of interest.

References

1. Shinar, J.; Savvateev, V. Introduction to organic light-emitting devices. In *Organic Light-Emitting Devices: A Survey*; Shinar, J., Ed.; Springer: New York, NY, USA, 2004; pp. 1–41.
2. Lee, J.; Park, Y.; Jung, J.; Han, W.-S. Blue-shifted aggregation-induced emission of siloles by simple structure modification and their application as nitro explosive chemosensors. *Photochem. Photobiol. Sci.* **2017**, *16*, 1495–1501. [[CrossRef](#)] [[PubMed](#)]
3. Yang, Y.; Zhao, Q.; Feng, W.; Li, F. Luminescent chemodosimeters for bioimaging. *Chem. Rev.* **2013**, *113*, 192–270. [[CrossRef](#)] [[PubMed](#)]
4. Luo, J.; Xie, Z.; Lam, J.W.Y.; Cheng, H.; Qui, C.; Kwok, H.S.; Zhan, X.; Liu, Y.; Zhu, D.; Tang, B.Z.; et al. Aggregation-induced emission of 1-methyl-1,2,3,4,5-pentaphenylsilole. *Chem. Commun.* **2001**, 1740–1741. [[CrossRef](#)] [[PubMed](#)]
5. Mei, J.; Leung, N.L.C.; Kwok, R.T.K.; Lam, J.W.Y.; Tang, B.Z. Aggregation-induced emission: Together we shine, united we soar! *Chem. Rev.* **2015**, *115*, 11718–11940. [[CrossRef](#)]
6. Pinto, A.; Svahn, N.; Lima, J.C.; Rodríguez, L. Aggregation induced emission of gold(I) complexes in water or water mixtures. *Dalton Trans.* **2017**, *46*, 11125–11139. [[CrossRef](#)]
7. Shu, T.; Wang, J.; Su, L.; Zhang, X. Luminescent organometallic nanomaterials with aggregation-induced emission. *Crit. Rev. Anal. Chem.* **2018**, *48*, 330–336. [[CrossRef](#)]
8. Zhang, J.; Zou, H.; Lei, J.; He, B.; He, X.; Sung, H.H.Y.; Kwok, R.T.K.; Lam, J.W.Y.; Zheng, L.; Tang, B.Z.; et al. Multifunctional Au^I-based AIEgens: Manipulating molecular structures and boosting specific cancer cell imaging and theranostics. *Angew. Chem. Int. Ed.* **2020**, *132*, 7163–7171. [[CrossRef](#)]
9. Chen, Z.; Zhang, J.; Song, M.; Yin, J.; Yu, G.-A.; Liu, S.H. A novel fluorene-based aggregation-induced emission (AIE)-active gold(I) complex with crystallization-induced emission enhancement (CIEE) and reversible mechanochromism characteristics. *Chem. Commun.* **2015**, *51*, 326–329. [[CrossRef](#)]
10. Yam, V.W.-W.; Au, V.K.-M.; Leung, S.Y.-L. Light-emitting self-assembled materials based on d⁸ and d¹⁰ transition metal complexes. *Chem. Rev.* **2015**, *115*, 7589–7728. [[CrossRef](#)]
11. Fujisawa, K.; Kawakami, N.; Onishi, Y.; Izumi, Y.; Tamai, S.; Sugimoto, N.; Tsutsumi, O. Photoluminescent properties of liquid crystalline gold(I) isocyanide complexes with a rod-like molecular structure. *J. Mater. Chem. C* **2013**, *1*, 5359–5366. [[CrossRef](#)]
12. Yamada, S.; Rokusha, Y.; Kawano, R.; Fujisawa, K.; Tsutsumi, O. Mesogenic gold complexes showing aggregation-induced enhancement of phosphorescence in both crystalline and liquid-crystalline phases. *Faraday Discuss.* **2017**, *196*, 269–283. [[CrossRef](#)] [[PubMed](#)]
13. Kuroda, Y.; Nakamura, S.; Srinivas, K.; Sathayanarayana, A.; Prabusankar, G.; Hisano, K.; Tsutsumi, O. Thermochemically stable liquid-crystalline gold(I) complexes showing enhanced room temperature phosphorescence. *Crystals* **2019**, *9*, 227. [[CrossRef](#)]
14. Tsutsumi, O.; Tamaru, M.; Nakasato, H.; Shimai, S.; Panthai, S.; Kuroda, Y.; Yamaguchi, K.; Fujisawa, K.; Hisano, K. Highly efficient aggregation-induced room-temperature phosphorescence with extremely large Stokes shift emitted from trinuclear gold(I) complex crystals. *Molecules* **2019**, *24*, 4606. [[CrossRef](#)] [[PubMed](#)]

15. Crespo, O. Gold–gold interactions. In *Modern Supramolecular Gold Chemistry: Gold-Metal Interactions and Applications*; Laguna, A., Ed.; Wiley-VCH: Weinheim, Germany, 2008; pp. 65–129.
16. Schmidbaur, H. The aurophilicity phenomenon: A decade of experimental findings, theoretical concepts and emerging applications. *Gold Bull.* **2000**, *33*, 3–10. [[CrossRef](#)]
17. Schmidbaur, H.; Schier, A. Aurophilic interactions as a subject of current research: An up-date. *Chem. Soc. Rev.* **2012**, *41*, 370–412. [[CrossRef](#)] [[PubMed](#)]
18. Baron, M.; Tubaro, C.; Biffis, A.; Basato, M.; Graiff, C.; Poater, A.; Cavallo, L.; Armaroli, N.; Accorsi, G. Blue-emitting dinuclear N-heterocyclic dicarbene gold(I) complex featuring a nearly unit quantum yield. *Inorg. Chem.* **2012**, *51*, 1178–1784. [[CrossRef](#)]
19. Lòpez-de-Luzuriaga, J.M. Luminescence of supramolecular gold-containing materials. In *Modern Supramolecular Gold Chemistry: Gold-Metal Interactions and Applications*; Laguna, A., Ed.; Wiley-VCH: Weinheim, Germany, 2008; pp. 347–401.
20. Kishimura, A.; Yamashita, T.; Aida, T. Phosphorescent organogels via “metallophilic” interactions for reversible RGB-color switching. *J. Am. Chem. Soc.* **2005**, *127*, 179–183. [[CrossRef](#)]
21. White-Morris, R.L.; Olmstead, M.M.; Attar, S.; Balch, A.L. Intermolecular interactions in polymorphs of trinuclear gold(I) complexes: Insight into the solvoluminescence of $\text{Au}^{\text{I}}_3(\text{MeN}=\text{COMe})_3$. *Inorg. Chem.* **2005**, *44*, 5021–5029. [[CrossRef](#)]
22. Balch, A.L.; Olmstead, M.M.; Vickery, J.C. Gold(I) compounds without significant aurophilic intermolecular interactions: Synthesis, structure, and electronic properties of $\text{Ph}_3\text{PAuC}(\text{O})\text{NHMe}$ and $\text{Au}_3(\text{PhCH}_2\text{N}=\text{COMe})_3$: Comparative monomeric and trimeric analogues of the solvoluminescent trimer, $\text{Au}_3(\text{MeN}=\text{COMe})_3$. *Inorg. Chem.* **1999**, *38*, 3494–3499.
23. Vickery, J.C.; Olmstead, M.M.; Fung, E.Y.; Balch, A.L. Solvent-stimulated luminescence from the supramolecular aggregation of a trinuclear gold(I) complex that displays extensive intermolecular $\text{Au}^{\text{I}}\text{Au}^{\text{I}}$ interactions. *Angew. Chem. Int. Ed. Engl.* **1997**, *36*, 1179–1181. [[CrossRef](#)]
24. Ito, H.; Saito, T.; Oshima, N.; Kitamura, N.; Ishizaka, S.; Hinatsu, Y.; Wakeshima, M.; Kato, M.; Tsuge, K.; Sawamura, M.; et al. Reversible mechanochromic luminescence of $[(\text{C}_6\text{F}_5\text{Au})_2(\mu\text{-}1,4\text{-diisocyanobenzene})]$. *J. Am. Chem. Soc.* **2008**, *130*, 10044–10045. [[CrossRef](#)] [[PubMed](#)]
25. Ito, H.; Muromoto, M.; Kurenuma, S.; Ishizaka, S.; Kitamura, N.; Sato, H.; Seki, T. Mechanical stimulation and solid seeding trigger single-crystal-to-single-crystal molecular domino transformations. *Nat. Commun.* **2013**, *4*, 2009. [[CrossRef](#)] [[PubMed](#)]
26. Seki, T.; Sakurada, K.; Muromoto, M.; Ito, H. Photoinduced single-crystal-to-single-crystal phase transition and photosalient effect of a gold(I) isocyanide complex with shortening of intermolecular aurophilic bonds. *Chem. Sci.* **2015**, *6*, 1491–1497. [[CrossRef](#)] [[PubMed](#)]
27. Seki, T.; Takamatsu, Y.; Ito, H. A screening approach for the discovery of mechanochromic gold(I) isocyanide complexes with crystal-to-crystal phase transitions. *J. Am. Chem. Soc.* **2016**, *138*, 6252–6260. [[CrossRef](#)] [[PubMed](#)]
28. Sathyanarayana, A.; Nakamura, S.; Hisano, K.; Tsutsumi, O.; Srinivas, K.; Prabusankar, G. Controlling the solid-state luminescence of gold(I) N-heterocyclic carbene complexes through changes in the structure of molecular aggregates. *Sci. China Chem.* **2018**, *61*, 957–965. [[CrossRef](#)]
29. Fujisawa, K.; Yamada, S.; Yanagi, Y.; Yoshioka, Y.; Kiyohara, A.; Tsutsumi, O. Tuning the photoluminescence of condensed-phase cyclic trinuclear Au(I) complexes through control of their aggregated structures by external stimuli. *Sci. Rep.* **2015**, *5*, 7934. [[CrossRef](#)]
30. Younis, O.; Rokusha, Y.; Sugimoto, N.; Fujisawa, K.; Yamada, S.; Tsutsumi, O. Effect of molecular structure and aggregated structure on photoluminescence properties of liquid-crystalline gold(I) complexes with various aromatic rings. *Mol. Cryst. Liq. Cryst.* **2015**, *617*, 21–31. [[CrossRef](#)]
31. Zhao, D. Liquid crystalline AIE luminogens: Properties and applications. In *Aggregation-Induced Emission: Materials and Applications*; Fujiki, M., Liu, B., Tang, B.Z., Eds.; ACS Symposium Series 1227; American Chemical Society: Washington, DC, USA, 2016; Volume 2, pp. 151–171.
32. Dai, S.; Cai, Z.; Peng, Z.; Wang, Z.; Tong, B.; Shi, J.; Gan, S.; He, Q.; Chen, W.; Dong, Y.; et al. A stabilized lamellar liquid crystalline phase with aggregation-induced emission features based on pyrrolopyrrole derivatives. *Mater. Chem. Front.* **2019**, *3*, 1105–1112. [[CrossRef](#)]

33. Guo, Y.; Shi, D.; Luo, Z.-W.; Xu, J.-R.; Li, M.-L.; Yang, L.-H.; Yu, Z.-Q.; Chen, E.-Q.; Xie, H.-L. High efficiency luminescent liquid crystalline polymers based on aggregation-induced emission and “jacketing” effect: Design, synthesis, photophysical property, and phase structure. *Macromolecules* **2017**, *50*, 9607–9616. [[CrossRef](#)]
34. Pucci, A. Mechanochromic fluorescent polymers with aggregation-induced emission features. *Sensors* **2019**, *19*, 4969. [[CrossRef](#)]
35. Sun, J.; Wang, J.; Chen, M.; Pu, X.; Wang, G.; Li, L.; Chen, G.; Cai, Y.; Gu, X.; Tang, B.Z.; et al. Fluorescence turn-on visualization of microscopic processes for self-healing gels by AIEgens and anticounterfeiting application. *Chem. Mater.* **2019**, *31*, 5683–5690. [[CrossRef](#)]
36. Tavakoli, J.; Pye, S.; Reza, A.H.M.M.; Xie, N.; Qin, J.; Raston, C.L.; Tang, B.Z.; Tang, Y. Tuning aggregation-induced emission nanoparticle properties under thin film formation. *Mater. Chem. Front.* **2020**, *4*, 537–545. [[CrossRef](#)]
37. Fujisawa, K.; Mitsushashi, F.; Anukul, P.; Taneki, K.; Younis, O.; Tsutsumi, O. Photoluminescence behavior of liquid-crystalline gold(I) complexes with a siloxane group controlled by molecular aggregate structures in condensed phases. *Polym. J.* **2018**, *50*, 761–769. [[CrossRef](#)]
38. Fujisawa, K.; Okuda, Y.; Izumi, Y.; Nagamatsu, A.; Rokusha, Y.; Sadaike, Y.; Tsutsumi, O. Reversible thermal-mode control of luminescence from liquid-crystalline gold(I) complexes. *J. Mater. Chem. C* **2014**, *2*, 3549–3555. [[CrossRef](#)]
39. Sun, F.; Zhange, G.; Zhang, D. A new gelator based on tetraphenylethylene and diphenylalanine: Gel formation and reversible fluorescence tuning. *Chin. Sci. Bull.* **2012**, *57*, 4284–4288. [[CrossRef](#)]
40. Yao, H.; Wang, J.; Song, S.-S.; Fan, Y.-Q.; Guan, X.-W.; Zhou, Q.; Wei, T.-B.; Lin, Q.; Zhang, Y.-M. A novel supramolecular AIE gel acts as a multi-analyte sensor array. *New J. Chem.* **2018**, *42*, 18059–18065. [[CrossRef](#)]
41. Aschmann, D.; Riebe, S.; Neumann, T.; Killa, D.; Ostwaldt, J.-E.; Wölper, C.; Schmuck, C.; Voskuhl, J. A stimuli responsive two component supramolecular hydrogelator with aggregation-induced emission properties. *Soft Matter* **2019**, *15*, 7117–7121. [[CrossRef](#)]
42. López, D.; García-Frutos, E.M. Aggregation-induced emission of organogels based on self-assembled 5-(4-nonylphenyl)-7-azaindoles. *Langmuir* **2015**, *31*, 8697–8702. [[CrossRef](#)]
43. Wang, M.; Zhang, D.; Zhang, G.; Zhu, D. Fluorescence enhancement upon gelation and thermally-driven fluorescence switches based on tetraphenylsilole-based organic gelators. *Chem. Phys. Lett.* **2009**, *475*, 64–67. [[CrossRef](#)]
44. Wang, X.; Ding, Z.; Ma, Y.; Zhang, Y.; Shang, H.; Jiang, S. Multi-stimuli responsive supramolecular gels based on a D- π -A structural cyanostilbene derivative with aggregation induced emission properties. *Soft Matter* **2019**, *15*, 1658–1665. [[CrossRef](#)]
45. Zhang, Y.; Liang, C.; Shang, H.; Ma, Y.; Jiang, S. Supramolecular organogels and nanowires based on a V-shaped cyanostilbene amide derivative with aggregation-induced emission (AIE) properties. *J. Mater. Chem. C* **2013**, *1*, 4472–4480. [[CrossRef](#)]
46. Externbrink, M.; Riebe, S.; Schmuck, C.; Voskuhl, J. A dual pH-responsive supramolecular gelator with aggregation-induced emission properties. *Soft Matter* **2018**, *14*, 6166–6170. [[CrossRef](#)] [[PubMed](#)]
47. Zhang, P.; Wang, H.; Liu, H.; Li, M. Fluorescence-enhanced organogels and mesomorphic superstructure based on hydrazine derivatives. *Langmuir* **2010**, *26*, 10183–10190. [[CrossRef](#)] [[PubMed](#)]
48. Babu, S.S.; Praveen, V.K.; Ajayaghosh, A. Function π -gelators and their applications. *Chem. Rev.* **2014**, *114*, 1973–2129. [[CrossRef](#)] [[PubMed](#)]
49. Gao, H.; Xue, P.; Peng, J.; Zhai, L.; Sun, M.; Sun, J.; Lu, R. Red-emitting dyes base on phenothiazine-modified 2-hydroxychalcone analogues: Mechanofluorochromism and gelation-induced emission enhancement. *New J. Chem.* **2019**, *43*, 77–84. [[CrossRef](#)]
50. Dou, C.; Chen, D.; Iqbal, J.; Yuan, Y.; Zhang, H.; Wang, Y. Multistimuli-responsive benzothiadiazole-cored phenylene vinylene derivative with nanoassembly properties. *Langmuir* **2011**, *27*, 6323–6329. [[CrossRef](#)] [[PubMed](#)]
51. Chung, J.W.; An, B.K.; Park, S.Y. A thermoreversible and proton-induced gel-sol phase transition with remarkable fluorescence variation. *Chem. Mater.* **2008**, *20*, 6750–6755. [[CrossRef](#)]
52. Luo, M.; Wang, S.; Li, C.; Miao, W.; Ma, X. Aggregation-induced emission organogel formed by both sonication and thermal processing base on tetraphenylethylene and cholesterol derivative. *Dye. Pigment.* **2019**, *165*, 436–443. [[CrossRef](#)]

53. Li, R.; Wang, S.; Li, Q.; Lan, H.; Xiao, S.; Li, Y.; Tan, R.; Yi, T. A fluorescent non-conventional organogelator with gelation-assisted piezochromic and fluoride-sensing properties. *Dye. Pigment.* **2017**, *137*, 111–116. [[CrossRef](#)]
54. Pang, X.; Yu, X.; Lan, H.; Ge, X.; Li, Y.; Zhen, X.; Yi, T. Visual recognition of aliphatic and aromatic amines using a fluorescent gel: Application of sonication-triggered organogel. *ACS Appl. Mater. Interfaces* **2015**, *24*, 13569–13577. [[CrossRef](#)]
55. Lui, K.; Meng, L.; Mo, S.; Zhang, M.; Mao, Y.; Cao, X.; Huang, C.; Yi, T. Colour change and luminescence enhancement in a cholesterol-based terpyridyl platinum metallogel via sonication. *J. Mater. Chem. C* **2013**, *1*, 1753–1762.
56. Ma, X.; Cui, Y.; Liu, S.; Wu, J. A thermos-responsive supramolecular gel and its luminescence enhancement induced by rare earth Y^{3+} . *Soft Matter* **2017**, *13*, 8027–8030. [[CrossRef](#)] [[PubMed](#)]
57. Wei, T.B.; Ma, X.Q.; Fan, Y.Q.; Jiang, X.M.; Dong, H.Q.; Yang, Q.Y.; Zhang, Y.F.; Yao, H.; Lin, Q.; Zhang, Y.M.; et al. Aggregation-induced emission supramolecular organic framework (AIE SOF) gels constructed from tri-pillar[5]arene-based foldamer for ultrasensitive detection and separation of multi-analytes. *Soft Matter* **2019**, *15*, 6753–6758. [[CrossRef](#)]
58. Hanabusa, K.; Yamada, M.; Kimura, M.; Shirai, H. Prominent gelation and chiral aggregation of alkylamides derived from *trans*-1,2-diaminocyclohexane. *Angew. Chem. Int. Ed. Engl.* **1996**, *35*, 1949–1951. [[CrossRef](#)]
59. Lima, J.C.; Rodríguez, L. Supramolecular gold metallogelators: The key role of metallophilic interactions. *Inorganics* **2015**, *3*, 1–18. [[CrossRef](#)]
60. Tam, A.Y.-Y.; Yam, V.W.-W. Recent advances in metallogels. *Chem. Soc. Rev.* **2013**, *42*, 1540–1567. [[CrossRef](#)]
61. Yuan, W.Z.; Shen, X.Y.; Zhao, H.; Lam, J.W.Y.; Tang, L.; Lu, P.; Wang, C.; Liu, Y.; Wang, Z.; Zheng, Q.; et al. Crystallization-induced phosphorescence of pure organic luminogens at room temperature. *J. Phys. Chem. C* **2010**, *114*, 6090–6099. [[CrossRef](#)]
62. Gong, Y.; Chen, G.; Peng, Q.; Yuan, W.Z.; Xie, Y.; Li, S.; Zhang, Y.; Tang, B.Z. Achieving persistent room temperature phosphorescence and remarkable mechanochromism from pure organic luminogens. *Adv. Mater.* **2015**, *27*, 6195–6201. [[CrossRef](#)]
63. Kawano, R.; Younis, O.; Ando, A.; Rokusha, Y.; Yamada, S.; Tsutsumi, O. Photoluminescence from Au(I) complexes exhibiting color sensitivity to the structure of the molecular aggregates. *Chem. Lett.* **2016**, *45*, 66–68. [[CrossRef](#)]



© 2020 by the authors. Licensee MDPI, Basel, Switzerland. This article is an open access article distributed under the terms and conditions of the Creative Commons Attribution (CC BY) license (<http://creativecommons.org/licenses/by/4.0/>).